CrossMark

The Relevance of Surface Roughness Data Qualities in Diagnostic Modeling of Wind Velocity in Complex Terrain: A Case Study from the Śnieżnik Massif (SW Poland)

Kacper Jancewicz[1] and Mariusz Szymanowski[1]

Abstract—Numerical modeling of wind velocity above complex terrain has become a subject of numerous contemporary studies. Regardless of the methodical approach (dynamic or diagnostic), it can be observed that information about surface roughness is indispensable to achieve realistic results. In this context, the current state of GIS and remote sensing development allows access to a number of datasets providing information about various properties of land coverage in a broad spectrum of spatial resolution. Hence, the quality of roughness information may vary depending on the properties of primary land coverage data. As a consequence, the results of the wind velocity modeling are affected by the accuracy and spatial resolution of roughness data. This paper describes further attempts to model wind velocity using the following sources of roughness information: LiDAR data (Digital Surface Model and Digital Terrain Model), database of topographical objects (BDOT10k) and both raster and vector versions of Corine Land Cover 2006 (CLC). The modeling was conducted in WindStation 4.0.2 software which is based on the computational fluid dynamics (CFD) diagnostic solver Canyon. Presented experiment concerns three episodes of relatively strong and constant synoptic forcing: 26 November 2011, 25 May 2012 and 26 May 2012. The modeling was performed in the spatial resolution of 50 and 100 m. Input anemological data were collected during field measurements while the atmosphere boundary layer parameters were derived from the meteorological stations closest to the study area. The model's performance was verified using leave-one-out cross-validation and calculation of error indices such as bias error, root mean square error and index of wind speed. Thus, it was possible to compare results of using roughness datasets of different type and resolution. The study demonstrates that the use of LiDAR-based roughness data may result in an improvement of the model's performance in 100 and 50 m resolution, comparing to CLC and BDOT10k. Furthermore, a slight improvement of these results can be accomplished if the LiDAR-based roughness calculation process includes the variable of prevailing wind direction. Qualities of both CLC and BDOT10k raw datasets (imposed land coverage classes, necessity of the roughness classes assignment) induce relatively high values of the modeled velocity error indices. Hence, these and other similar datasets need to be carefully analyzed (e.g. compared with aerial or satellite imagery) before they are used in the process of roughness length parameterization.

1. Introduction

Proper surface roughness estimation is considered as one of the most important aspects of microscale and mesoscale meteorological modeling (Hansen 1993; Emeis and Knoche 2007). Regardless of the methodical approach (dynamic or diagnostic) it can be assumed that roughness input data significantly affects results of the near-ground wind velocity modeling; only proper roughness parameterization may result in a realistic spatial distribution of modeled wind velocity. Hence, preparation of the input roughness dataset involves consideration of two issues: a method of roughness estimation and properties of the source of information.

The aerodynamic surface roughness z_0 value is the height above a surface at which the logarithmic profile of wind speed versus altitude extrapolates to zero wind speed (Jacobson 2005). Under neutral conditions, the idealized near-surface wind velocity profile can be expressed as:

$$u(z) = \frac{u_*}{\kappa} \ln\left(\frac{z}{z_0}\right) \qquad (1)$$

where u_* denotes friction velocity, κ von Karman's constant ($\kappa = 0.4$), z height above reference plane and z_0 aerodynamic surface roughness length (Emeis and Knoche 2007). The z_0 value can be treated as a fixed property of the surface; it is usually derived from measured wind profiles. The empirical estimation of roughness length has been considered by many authors since 1950s for both natural and

---

[1] Institute of Geography and Regional Development, University of Wrocław, pl. Uniwersytecki 1, 50-137 Wrocław, Poland. E-mail: kacper.jancewicz@uni.wroc.pl

anthropogenic surfaces. Hence, some analyses consist of exhaustive lists of z_0 values assigned to specific forms of land coverage (e.g. HANSEN 1993; CHO et al. 2012). A detailed review of roughness data from boundary-layer experiments was provided by WIERINGA (1993), who stated that the classification created by DAVENPORT (1960) describes roughness of landscape types in the most reliable way. After several updates (WIERINGA et al. 2001), it has become probably the best field-validated roughness classification to date (HAMMOND et al. 2012) (Appendix 1).

On the other hand, numerous authors have focused on the relation between z_0 value and parameters of surface obstacles. This approach resulted in a broad range of roughness definitions. For instance, roughness length can be described simply as a function of surface objects height (e.g. PLATE 1982; GARRATT 1994; LOPES 2013):

$$z_0 = fh_c \tag{2}$$

where h_c denotes height of the roughness element. The f value of 0.15 is recommended for most natural surfaces (PLATE 1982). In fact, it depends on the layout and shape of roughness elements. Hence, the f range is variously specified, depending on the author, e.g. 0.03–0.25 (LOPES 2013) or 0.07–0.14 (GARRATT 1994). Subsequently, the exploration of properties of roughness elements (and their relation to z_0) resulted in the inclusion of much more sophisticated morphometric analyses in the process of surface roughness estimation. These methods are usually applied in order to determine aerodynamic parameters of dense urban areas, where empirical anemometric estimation of z_0 may not give sufficient results or is impossible to perform (GRIMMOND and OKE 1999; SUDER and SZYMANOWSKI 2014).

Direct application of the logarithmic law (Eq. 1) encounters difficulties in the areas which are densely built-up or covered by high vegetation. Thus, an additional parameter, a zero-plane displacement height (d), was added to roughness description (THOM 1971; JACKSON 1981), resulting in:

$$u(z) = \frac{u_*}{\kappa} \ln\left(\frac{z-d}{z_0}\right) \tag{3}$$

where d value can be regarded as a datum height above which normal turbulent exchange takes place

(HANSEN 1993). It is comparable to the depth of an air layer trapped in vegetation (or in urban structure) and depends on the density of the obstacles—the d becomes negligible when they are sparsely distributed (WIERINGA 1993). However, some authors raise the controversial aspect of the zero-plane displacement, stating that much information concerned with d can be included in z_0 by increasing its value (DONG et al. 2001).

Aforementioned roughness parameters refer only to homogenous surfaces. In practice, the single grid cell of the numerical flow model usually represents heterogeneous land use, which should be parameterized by the effective roughness length z_{0eff} (EMEIS and KNOCHE 2007). According to TAYLOR (1987), the z_{0eff} can be approximated by an ensemble average of local z_0 values inside the grid cell. A different approach was proposed by YAMAZAWA and KONDO (1989) who considered that z_{0eff} should be calculated for the windward fetch areas which was a wedge with $45°$ angle and a radius $R = 100\, h_a$ (where h_a denotes height of the anemometer placement). Similarly, HAMMOND et al. (2012) calculated z_{0eff} as an arithmetic average of z_0 values within fans of various radius lengths (from 100 to 500 m).

An utterly different concept of surface drag parameterization concerns sub-grid scale orographic effects (WOOD et al. 2001, JIMENEZ and DUDHIA 2012). In reality, orography is not uniform—there are concave and convex terrain forms which are too small to be represented explicitly within a single grid of assumed resolution. Hence, additional parameterization (of momentum equation) should be made in order to include terrain characteristics inside every grid. This problem applies mainly to mesoscale meteorological models—a fine example is provided by JIMENEZ and DUDHIA (2012), who demonstrate improvements of WRF model's performance (resolution—2 km) by use of the standard deviation of the subgrid-scale orography as well as the Laplacian of the topographic field.

In reference to the aforementioned methodical background, it is possible to focus on potential sources of information about roughness. The current state of remote-sensing techniques and GIS systems development allows one to access a number of datasets from which roughness length z_0 can be

derived. They can be, in general, classified into four categories—three of which are remote-sensing-based (Table 1).

The first two groups of datasets provide information about distribution of land-coverage types inside the selected area. Thus, the values of surface roughness length (z_0) can be assigned to the consecutive land-coverage classes. Therefore, the quality of roughness information depends on the initial data resolution, the number of included land-use types and the accuracy of assignment of roughness length values. The last issue is considerably dependent upon the choice of appropriate roughness values from those proposed by various authors (e.g. Corine Land Cover roughness length values—SILVA *et al.* 2007). Regardless of the processing issues, an unquestionable advantage of these datasets is their accessibility.

The third group of datasets—the multi-spectral satellite images—allows to parameterize roughness as a derivative of vegetation indices, calculated from the bands of particular spectrum. For instance, the use of the normalised difference vegetation index (NDVI) (RAMLI *et al.* 2009) and the leaf area index (LAI) (SCHAUDT and DICKINSON 2000) to calculate z_0 should be mentioned in this context.

The last group contains high-resolution digital surface models (DSMs) and digital terrain models (DTMs). They are usually derived from data gathered by the airborne light detection and ranging (LiDAR) devices. Subtracting DTM from DSM results in a dataset containing a height of surface objects (h_c from

the Eq. 2) (HAMMOND *et al.* 2012). In consequence it is possible to estimate z_0 values within very high (2 m or less) resolution and then recalculate it into z_{0eff} which represents a surface appropriate to model grid size. Another advantage of LiDAR-based data is the fact that obtained z_0 has a continuous form. Thus, it should give much better approximation of real surface properties than pre-classified land-cover data.

In consequence, the present authors intend to consider how the properties and the quality of roughness data affect the results of the wind velocity modeling. The starting point is a recent research on using the CLC data in a case study of near ground wind field diagnostic modeling (solver: Canyon, LOPES 2003) in mountainous terrain. JANCEWICZ (2014) demonstrated that including CLC-derived input roughness information generally adjusts model's performance, comparing to the results achieved with spatially-uniform roughness (root mean squared error of velocity = 1.0 m/s instead of 1.6 m/s). However, he also concluded that raw CLC data may generate incorrect spatial distribution of roughness values due to the terrain complexity. Therefore, one could cautiously suppose that the use of a more detailed (or higher-quality) source of roughness information may further improve the performance of the model. An opportunity of using airborne LiDAR-derived data and a detailed topographical database is, in that case, especially promising.

This study concerns continued attempts of wind-field modeling in a part of the Śnieżnik Massif, which

Table 1

Main sources of data used in the roughness length estimation

| Data type	Examples of studies concerning roughness determination or wind velocity modelling
Land-use components of vector topographic databases	*Top10DK*: HASAGER *et al.* (2003)
Remote-sensing-based land coverage qualitative datasets	*Corine Land Cover*
	HASAGER *et al.* (2003), SILVA *et al.* (2007), TRUHETZ (2010), JANCEWICZ (2014) and DE MEIJ and VINUESA (2014)
	Global land cover characterization
	MORALES *et al.* (2012)
Multi-spectral satellite images	*Landsat TM*: JASINSKI and CRAGO (1999) and RAMLI *et al.* (2009)
	SPOT-5 TIAN *et al.* (2011)
	NOAA-AVHRR: SCHAUDT and DICKINSON (2000)
Remote-sensing-based high-resolution digital surface models (DSMs) and digital terrain models (DTMs)	*Airborne LiDAR-based DSM and DTM* COLIN and FAIVRE (2010), TIAN *et al.* (2011) and HAMMOND *et al.* (2012)
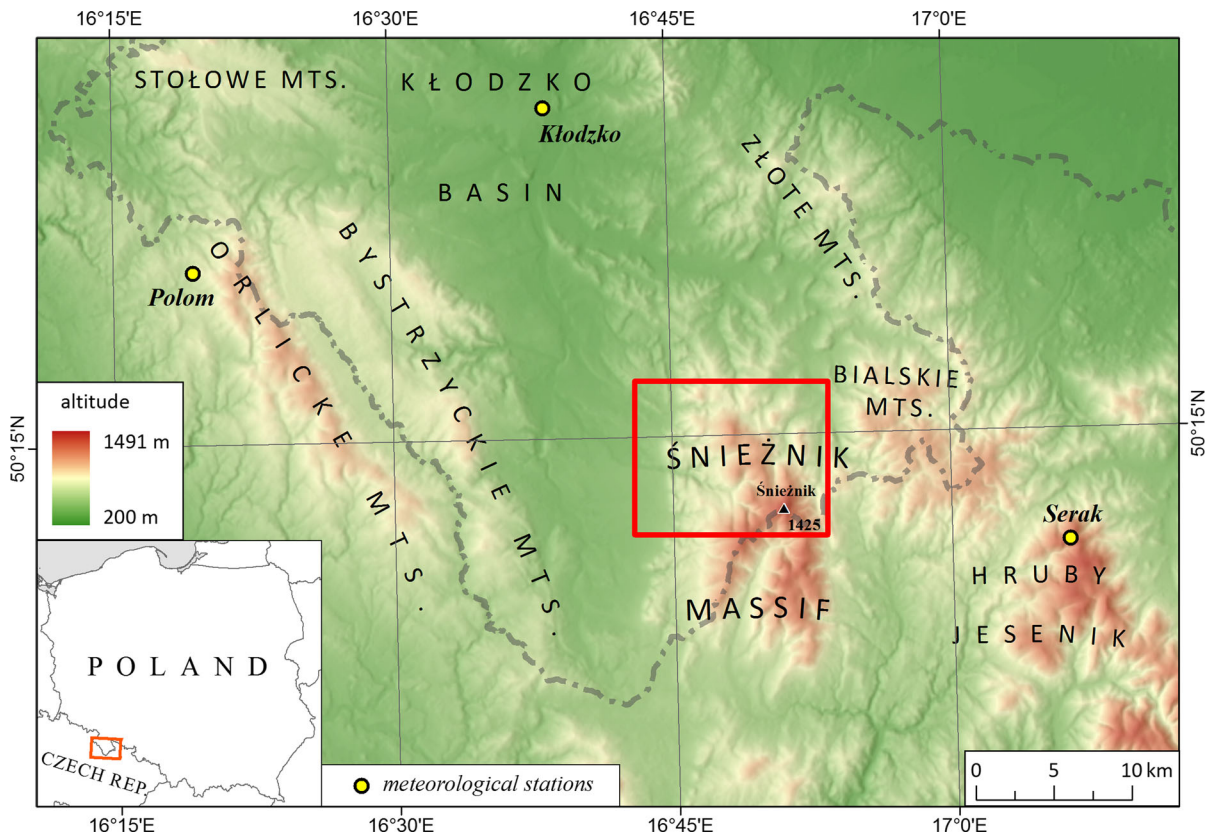
Figure 1
Position of the study area (marked by the *red rectangle*)

were undertaken in order to settle an issue of the potential impact of roughness data properties (resolution, data type) on the results of near-ground wind velocity diagnostic modeling.

2. Study Area

The Śnieżnik Massif, divided by the border of Poland and the Czech Republic (known there as Králický Sněžník) (Fig. 1), is the second highest mountain terrain in the Eastern Sudetes. The highest peak of the massif is Śnieżnik (1425 m a.s.l.). The massif itself represents a prominent orographic barrier, as it is surrounded by valleys and basins. Therefore, its morphology, containing deep valleys and long ridges (altitude range 1100–1300 m a.s.l.), causes local deformations of air flow. Prevailing wind directions are W, SW, S. If they are combined with strong synoptic forcing, then air-flows follow valley axes in the windward part of the massif. If conditions are favourable, foehn winds occur and the adaptation of flow direction may be also observed in leeward valleys (PIASECKI 1996; PIASECKI and SAWIŃSKI 2009).

Since 2011, the Śnieżnik Massif has been an area of studies focused on diagnostic modeling of near-ground air-flow using GIS techniques and remote-sensing data (JANCEWICZ 2014). The research polygon covers an area of 120 sq km in the north-western part of the massif (Fig. 1); within this area the altitude varies from 421 to 1425 m a.s.l. A detailed map of this area is presented on Fig. 2.

3. Methods

The modeling process was carried out using WindStation 4.0.2 software. It is based on the CFD
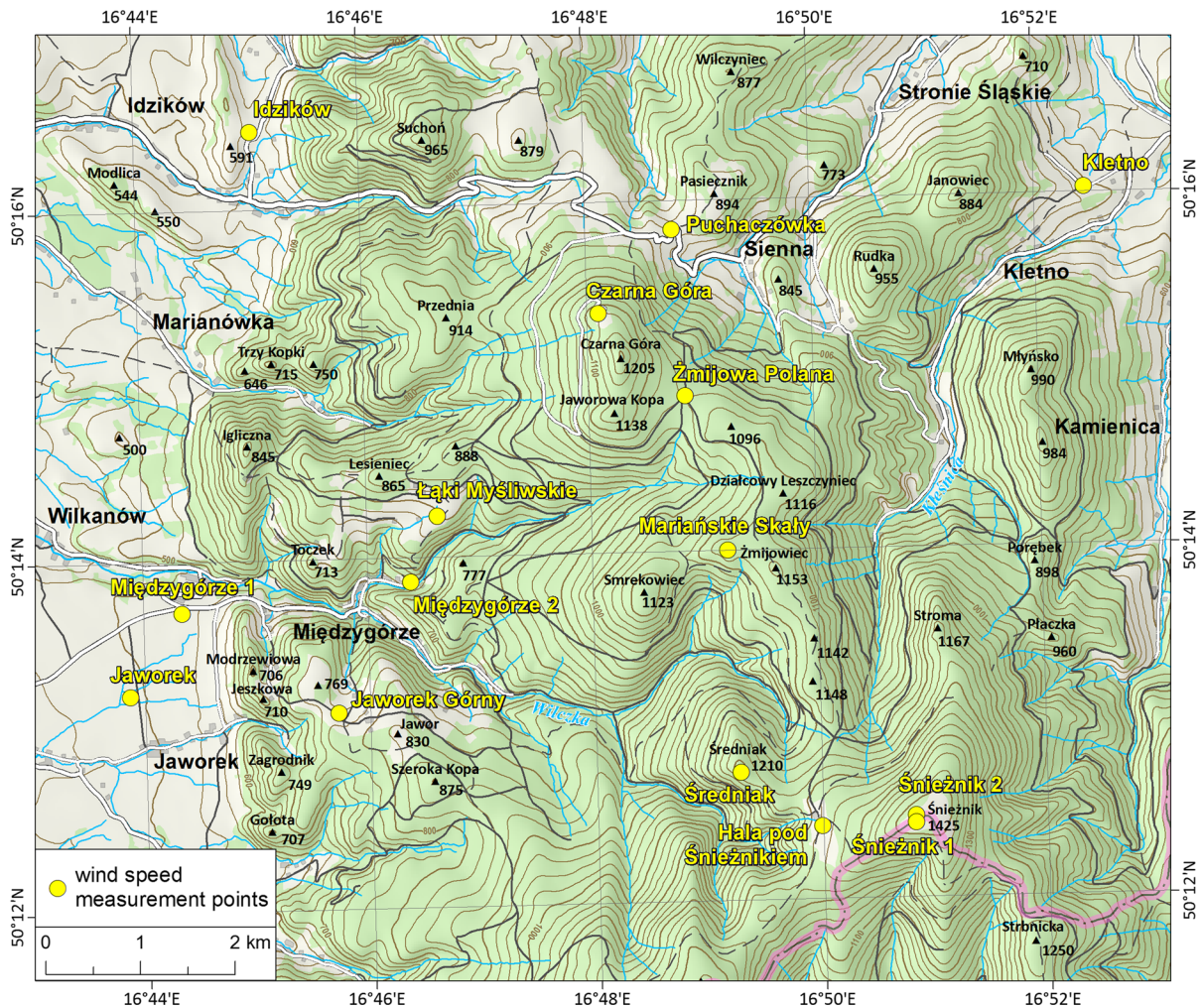
Figure 2
Distribution of wind measurement points inside the study area (after JANCEWICZ 2014)

solver Canyon, which solves for mass conservation, momentum conservation (Navier–Stokes equations), energy conservation and turbulence quantities (k–ε model) (LOPES 2003, 2013). The first version of WindStation was presented in 2003—its performance was validated using data obtained from the Askervein Hill site and two test areas in Portugal (LOPES 2003). Later versions were used in several studies. COLIN and FAIVRE (2010) applied Canyon in the process of aerodynamic roughness length estimation in Heihe basin (China), using high-resolution LiDAR elevation data. ABBES and BELHADJ (2012) used it to estimate resources of wind energy in the El-Kef region

(Tunisia). Eventually, Canyon solver was used by JANCEWICZ (2014) in an experiment concerning the modeling of near-ground wind velocity and direction at the test-site in the Śnieżnik Massif (SW Poland).

The input anemological data were obtained during short periods (6 h a day—from 9:00 to 15:00 CET/CEST)—velocity measurements were taken at a height of 2 m above ground at 5 min intervals, using Kaindl Windmaster 2 anemometers. Wind direction was estimated to the nearest of the 16 points of the compass as a result of observation of banners mounted on poles—in accordance with official guidelines (WMO 2008). Spatial distribution and the

Table 2

Measurement points used in the wind velocity modeling case study (after JANCEWICZ 2014)

ID	Measurement point	λ	φ	Altitude (m)	26-11-2011		25-05-2012		26-05-2012	
					Mean V (m/s)	Mean direction	Mean V (m/s)	Mean direction	Mean V (m/s)	Mean direction
1	Czarna Góra	16°48′06.3″E	50°15′21.9″N	1122	–	–	–	–	2.6	45
2	Hala p. Śnieżnikiem	16°49′59.6″E	50°12′24.9″N	1229	3.6	270	3.5	0	–	–
3	Idzików	16°45′03.2″E	50°16′26.9″N	567	–	–	–	–	4.1	0
6	Jaworek	16°43′52.3″E	50°13′14.3″N	494	–	–	4.3	7.5	–	–
4	Jaworek Górny	16°45′42.7″E	50°13′07.5″N	759	–	–	–	–	3.6	7.5
5	Kletno	16°52′26.8″E	50°16′01.7″N	611	–	–	4.7	348.8	–	–
7	Łąki Myśliwskie	16°46′37.6″E	50°14′14.0″N	795	1.3	247.5	–	–	2.8	45
8	Mariańskie Skały	16°49′12.4″E	50°14′00.1″N	1133	3.9	225	–	–	4.8	22.5
9	Międzygórze 1	16°44′20.8″E	50°13′42.6″N	520	2.8	202.5	2.2	0	–	–
10	Międzygórze 2	16°46′23.1″E	50°13′51.8″N	636	–	–	–	–	1.7	191.3
11	Puchaczówka	16°48′46.4″E	50°15′50.3″N	868	–	–	3.3	45	–	–
12	Śnieżnik 1	16°50′49.5″E	50°12′25.5″N	1424	3.5	213.8	–	–	–	–
13	Śnieżnik 2	16°50′49.6″E	50°12′28.1″N	1423	–	–	9.0	22.5	–	–
14	Średniak	16°49′16.7″E	50°12′43.9″N	1199	5.5	247.5	4.2	22.5	–	–
15	Żmijowa Polana	16°48′51.4″E	50°14′53.1″N	1047	2.8	202.5	–	–	3.2	22.5

list of measurement points are presented respectively in Fig. 2 and Table 2. This distribution pattern of anemometers was premeditated—the velocity was recorded within a broad range of altitude, relative exposure to mean wind direction, yet in the locations of minimized screening by topographic objects or vegetation (except Czarna Góra and Międzygórze 2 sites—JANCEWICZ 2014).

Similarly to the previous study, the experiment presented here concerns three episodes of relatively strong and constant synoptic forcing: 26 November 2011, 25 May 2012 and 26 May 2012 (Fig. 3). Differences between the velocity ratio at Kłodzko and Mt Šerak synoptic stations (Fig. 1) (JANCEWICZ 2014) can be partly explained by prevailing wind direction (November—WNW, both May days—NE/NNE), also diurnal local convection should be considered during May episode. A slow decrement of wind velocity on Mt Šerak (May 26, Fig. 3c) may also be a consequence of gradual weakening of horizontal pressure gradient. However, field measurements did not indicate such changes of velocity ratio between

points placed at high and low altitudes during measurement periods. In consequence, these 3 days were recognized as the most suitable for further modeling regarding vices and virtues of the diagnostic solver.

Further anemological data preparation involved calculation of hourly mean velocity values and prevailing directions in order to create an input dataset for the model. Wind conditions from the upper parts of the atmospheric boundary layer were obtained from upper air soundings performed in stations nearest to the study area: Prague-Libus, Prostějov and Wrocław. Those stations are relatively far from the study area, nevertheless the mean values of upper wind velocity and direction had to be introduced as the only available approximation. The results of the soundings were provided by the Department of Atmospheric Science at the University of Wyoming (http://www.weather.uwyo.edu/upperair/sounding.html, access date: June 10, 2012).

The second component of the input data was a LiDAR-based high resolution (1 m) Digital Terrain Model (DTM)—a product of IT System of the
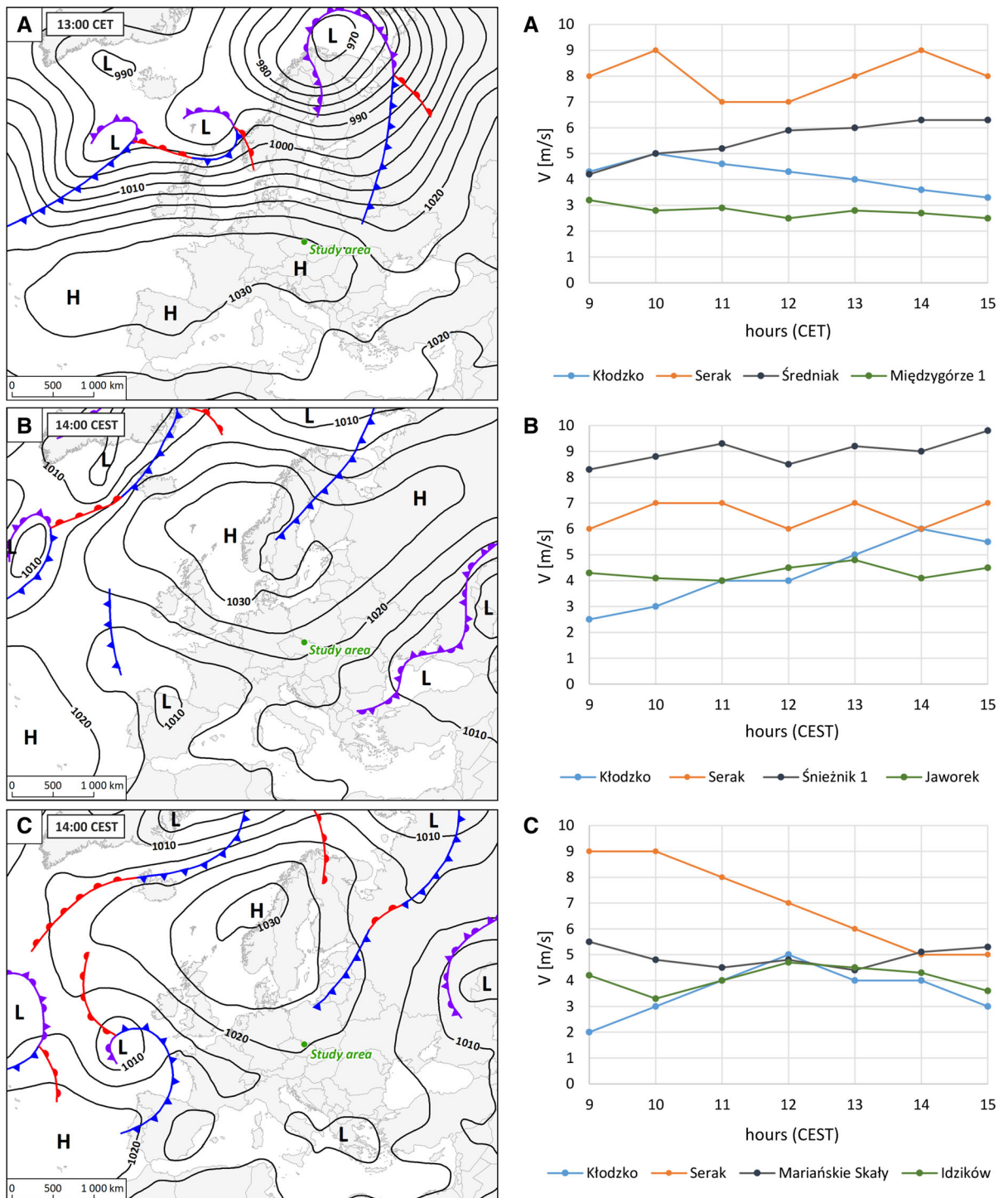
Figure 3
Atmospheric pressure field over Europe (*left*) and wind velocity observed within study area and in Serak and Kłodzko synoptic stations (*right*) during measurement time-periods : **a** 26 November 2011; **b** 25 May 2012; **c** 26 May 2012 (after JANCEWICZ 2014)

Table 3

Roughness classes assigned to CLC and BDOT10k datasets

Land-use class names	z_0 (m)	h_c (m)	% of total area		
			CLC (raster)	CLC (vector)	BDOT 10k
Inland water	0.0	0.0	0.0	0.0	0.1
Bare rock; dump sites; mineral extraction sites	0.01	0.07	0.0	0.0	0.2
Natural grasslands; non-irrigated arable land; pastures	0.03	0.2	17.4	17.2	24.3
Roads and associated land	0.04	0.3	0.0	0.0	0.2
Complex cultivation patterns; land principally occupied by agriculture with significant areas of natural vegetation	0.1	0.7	9.9	10.0	0.0
Sparsely vegetated areas	0.2	1.3	0.0	0.0	0.2
Agro-forestry areas; construction sites; fruit trees and berry plantations; green urban areas	0.3	2.0	0.0	0.0	1.3
Transitional woodland-shrub	0.4	2.7	7.2	7.2	1.1
Discontinuous urban fabric	0.6	4.0	1.4	1.4	1.0
Broad leaved forest; coniferous forest; mixed forest	1.4	9.3	64.0	64.2	71.5
Continuous urban fabric	1.5	10.0	0.0	0.0	0.1

Country's protection against extreme hazards (ISOK) Project (http://www.isok.gov.pl/en/products-of-isok-project, access date: May 30th, 2015). The model was resampled using cubic convolution method to 100 and 50 m in order to fit the settings of calculation domain.

The third input data component contained roughness information derived from four different datasets:

1. Corine Land Cover 2006 raster dataset (CLC_R) (version 15) (2011)—100 m resolution, provided by the European Environmental Agency (EEA);
2. Corine Land Cover 2006 vector dataset (CLC_V) (version 17) (2013)—provided by EEA;
3. Database of topographical objects (BDOT10k)— vector database, corresponding to topographic map scale 1:10,000—provided by the Polish Head Office of Geodesy and Cartography.
4. LiDAR-based DSM and DTM, spatial resolution: 1 m, provided by the Polish Head Office of Geodesy and Cartography.

Due to different properties, each dataset had to be individually pre-processed in order to fit the domain's resolution and to provide input roughness information required by WindStation—the height of surface objects (h_c). Thus, the CLC_R data were resampled to 50 m with use of the majority technique, while CLC_V

and BDOT10k were converted to raster format in the appropriate resolutions using maximum combined area approach (in consequence, the raster values reflected a dominant type of land coverage inside every cell). The next step was assignment of roughness length, which was based on the Finnish Wind Atlas (http://www.tuuliatlas.fi/modeling/mallinnus_3.html, access date: March 20th, 2014) and SILVA et al. (2007). In the case of BDOT10k, original land use classes had to be matched with CLC classification. Finally, the assigned z_0 values allowed calculating the h_c values according to the transformed Eq. 2 (PLATE 1982; LOPES 2013):

$$h_c = \frac{z_0}{0.15} \qquad (4)$$

The results of the roughness classes' assignment are presented in Table 3.

A different approach was required in case of LiDAR data. Firstly, the h_c was calculated, with reference to HAMMOND et al. (2012):

$$h_c = 0.6(\text{DSM} - \text{DTM}) \qquad (5)$$

where 0.6 is the value of porosity factor P (HEISLER and DEWALLE 1988) and approximates the porosity of forest canopy. Secondly, the initial h_c raster was recalculated to obtain mean values of h_c for every 50 and 100 m grid.
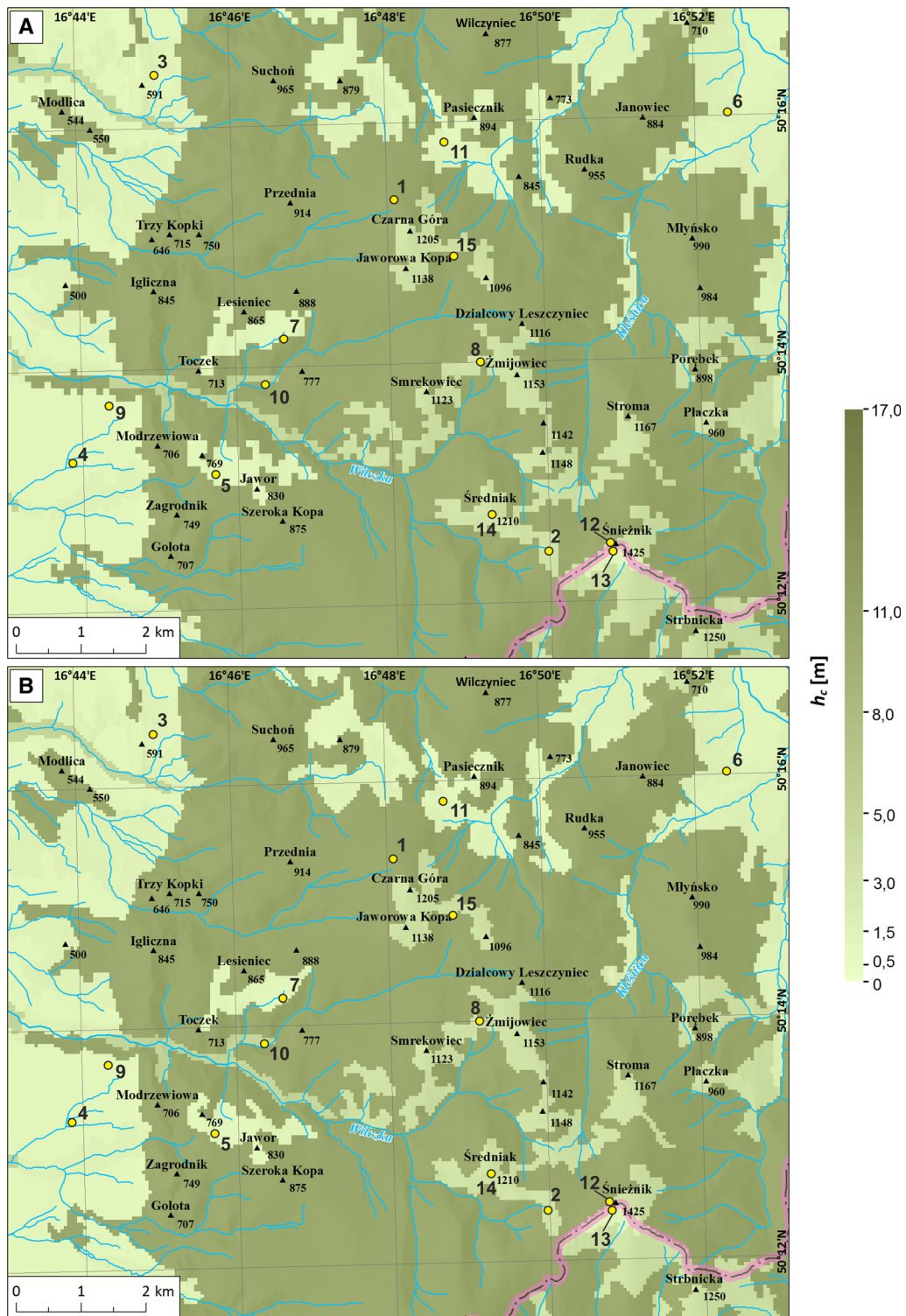
Figure 4
Distribution of the height of surface objects (h_c) inside the study area, according to the: **a** CLC raster version, **b** CLC vector version. *Yellow dots* indicate measurement/validation points
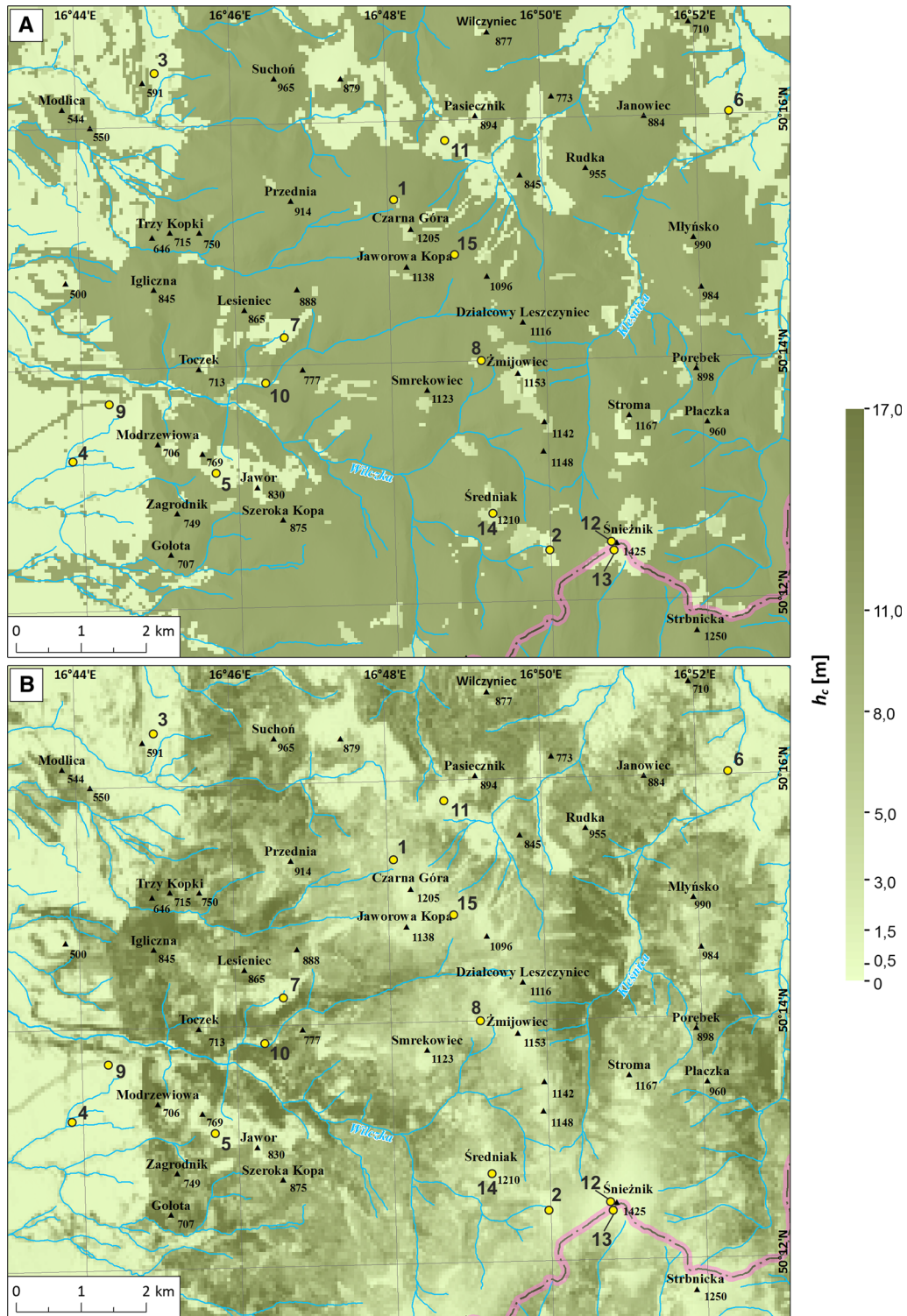
Figure 5
Distribution of the height of surface objects (h_c) inside the study area, according to the: **a** BDOT10k vector database, **b** LiDAR-based DEM and DSM. *Yellow dots* indicate measurement/validation points
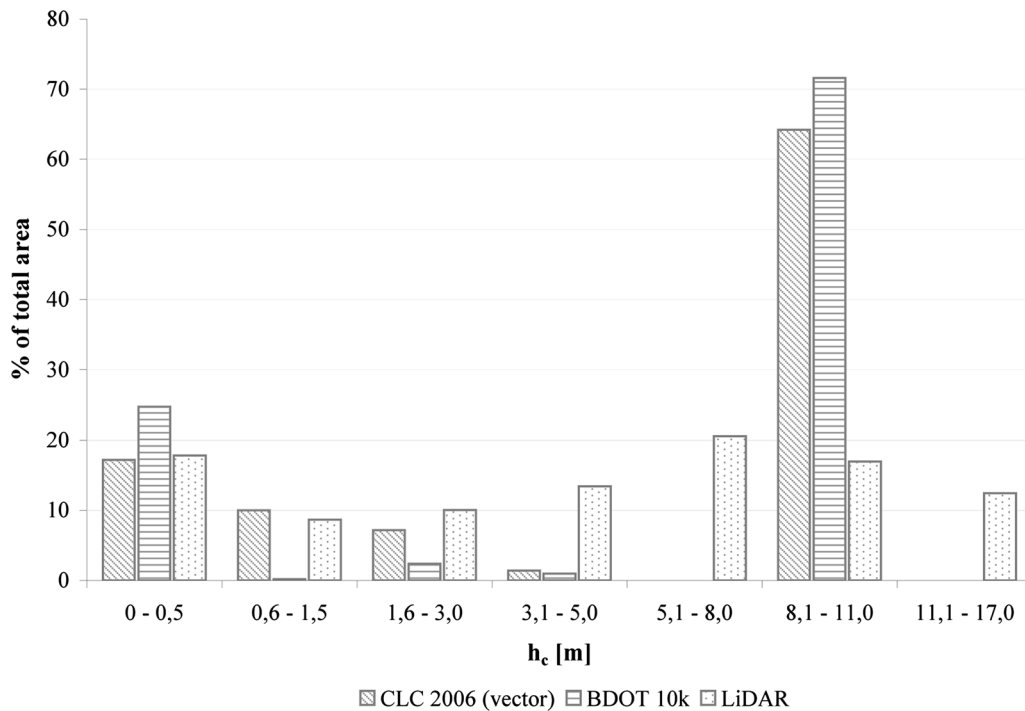
Figure 6
Percentage share of roughness parameter h_c classes inside the study area, depending on the initial source of roughness information

The results of the foregoing procedure are presented on roughness maps (Figs. 4, 5), which clearly demonstrate how the spatial distribution of roughness can differ according to the source's properties. Unsurprisingly, the LiDAR data provided the most detailed and realistic spatial distribution of h_c (Fig. 5), reflecting gradual decrease of forest vegetation height towards higher altitudes. This phenomenon is shown by neither CLC_R, CLC_V nor BDOT10k, which rely on an average roughness value for "forest" class. However, both CLC datasets include class of "transitional woodland-shrub", which gives lower roughness values on the ridges (Table 3; Fig. 4), while BDOT10k presents forest as completely uniform. On the other hand, this dataset provides (comparing to both CLCs) a much more detailed spatial distribution of roughness elements in the areas dominated by agricultural or post-agricultural land-use forms (Fig. 5). Overall, the different ways of representing roughness of forested areas by particular datasets cause significant differences among the range of high roughness values (Fig. 6).

The aforesaid roughness data were calculated according to the Taylor's (1987) concept of effective roughness length, which is insensitive to the variable of wind direction. However, the authors also recalculated h_c values of LiDAR data basing on the upwind fetch approach (Yamazawa and Kondo 1989; Hammond et al. 2012). This resulted in "windward effective h_c" ($h_{c\text{eff}}$) which is a mean value for fans of 45° angle, 200 m radius from the initial cell and the azimuth value matched to the wind direction which was prevailing during the modeled episode.

Eventually, modeling was conducted, using consecutively four prepared roughness datasets. The computational grid had $292 \times 252 \times 20$ nodes, with the first node placed at 4 m. Similarly to the previous studies (Lopes 2003; Jancewicz 2014), a neutral atmospheric stability was assumed. This decision was supported by analyses of aerological soundings conducted at stations in Wrocław, Prague and Prostějov. Again, it should be emphasized that those are the *nearest* stations, yet they are still very far from the study area (ca. 100 km). Hence, the results of

soundings cannot be uncritically considered as a source of detailed information on vertical changes of atmospheric stability within the calculation domain. Furthermore, the model setup requires choosing between stable, neutral or unstable conditions for an entire altitude range of the domain. In these circumstances, an assumption of neutral conditions seems to be a justified simplification. Nonetheless, while interpreting the results of modeling, one should consider possible occurrence of shallow layers characterized by low values of temperature gradient (or even thermal inversion), especially on 26 November 2011, though it is not explicitly indicated by wind velocity field measurements nor background data from stations at Kłodzko and Mt Šerak. Consequently, the results and the following conclusions apply only to the aforesaid assumptions.

Raw output data were converted to a point vector layer and, subsequently, to a raster format using the spline interpolation method. Additionally, the mean velocity was calculated for selected hours and different roughness data setups; this calculation based on the raster representations of wind velocity at 2 m above ground, which were a result of the model's consecutive runs. Finally, it was possible to present examples of spatial variability of modeled velocity and to compare the effects of using different roughness datasets.

The model's performance was evaluated through the execution of a modified leave-one-out cross-validation. The measured wind velocity data served as a base to create two subsets ("training" data and validation data). Per every observational hour, 20 different training datasets were randomly chosen with the stipulation that all of them had to contain at least

two measurement points. In consequence, 120 runs of the model were performed per every day and roughness setup (Jancewicz 2014). As a result, the following indices were calculated: velocity Bias (B_v), root mean square error of velocity ($RMSE_v$), index of wind speed (I_v); the equations are presented in Table 4.

4. Results and Discussion

The procedure applied created possibility to compare spatial differences between near-ground wind-velocity fields, which were calculated on the basis of different roughness input data. Examples of velocity maps are presented on Figs. 7, 8 and 9, while maps presenting the spatial distribution of mean velocity differences are displayed on Figs. 10 and 11. It becomes clear that the spatial variability of velocity strongly reflects the distribution of h_c parameter (see roughness maps in Figs. 4, 5). Therefore, it is not surprising that the use of CLC_R and CLC_V roughness data yielded very similar wind-fields (Fig. 7)—some slight differences may be noticed only if the boundaries of land-use classes differ in location due to the properties (raster/vector) of the initial datasets. Fine examples of these differences can be observed on the northern slopes of Jawor peak (SW part of the study area) or on the slopes of Średniak and Żmijowiec (Fig. 10a).

The use of BDOT10k roughness resulted in a wind-field characterized by relatively low velocities above ridges and peaks at altitude of 1000–1300 m a.s.l. (e.g. Żmijowiec, Czarna Góra and southern slopes of Śnieżnik) (Fig. 10b). This is because

Table 4

Error measures used in evaluation of overall wind velocity modeling results

Variable	Error measure	Equation	Remarks
Wind velocity	Bias error (Emery *et al.* 2001)	$B_v = \frac{1}{N} \sum_{i=1}^{N} (v_m - v_o)$	v_m—Modelled wind velocity v_o—Observed wind velocity
	Root mean square error (Emery *et al.* 2001)	$RMSE_v = \sqrt{\frac{1}{N} \sum_{i=1}^{N} (v_m - v_o)^2}$	v_m—Modelled wind velocity v_o—Observed wind velocity
	Index of wind speed Lopes (2003)	$I_v = \frac{1}{N} \sum_{i=1}^{N} 100e^{\left[-0.692\left(\frac{v_1}{v_2}-1\right)\right]}$	v_1, v_2—Observed and simulated velocities or vice versa, with $v_1 > v_2$

Figure 7
Spatial distribution of mean modeled wind velocity at height of 2 m above ground (26 May 2012; 13:00); roughness length information derived from: **a** CLC raster version, **b** CLC vector version. The velocity values were calculated from the results of 20 simulations based on various combinations of the input measurement points (containing at least two points). *Yellow dots* indicate measurement/validation points, *numbers* indicate point ID—see Tables 2 and 5
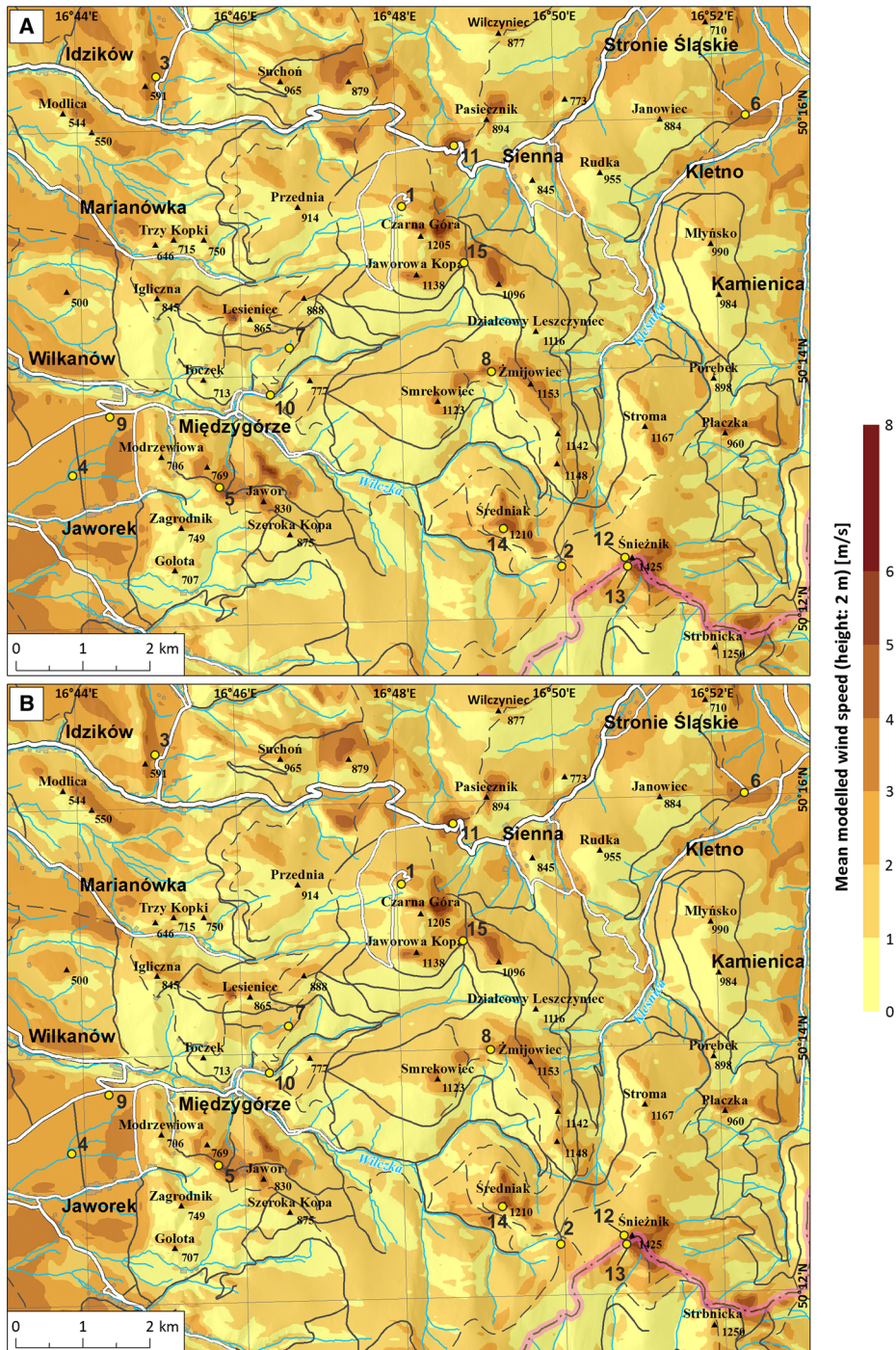
Figure 8
Spatial distribution of mean modeled wind velocity at height of 2 m above ground (26 May 2012; 13:00); roughness length information derived from: **a** BDOT10k vector database, **b** LiDAR-based DEM and DSM. The velocity values were calculated from the results of 20 simulations based on various combinations of the input measurement points (containing at least two points). *Yellow dots* indicate measurement/validation points, *numbers* indicate point ID—see Tables 2 and 5

Figure 9
Spatial distribution of mean modeled wind velocity at height of 2 m above ground (26 November 2011; 13:00); roughness length information derived from: **a** BDOT10k vector database, **b** LiDAR-based DEM and DSM. The velocity values were calculated from the results of 20 simulations based on various combinations of the input measurement points (containing at least two points). *Yellow dots* indicate measurement/validation points, *numbers* indicate point ID—see Tables 2 and 5
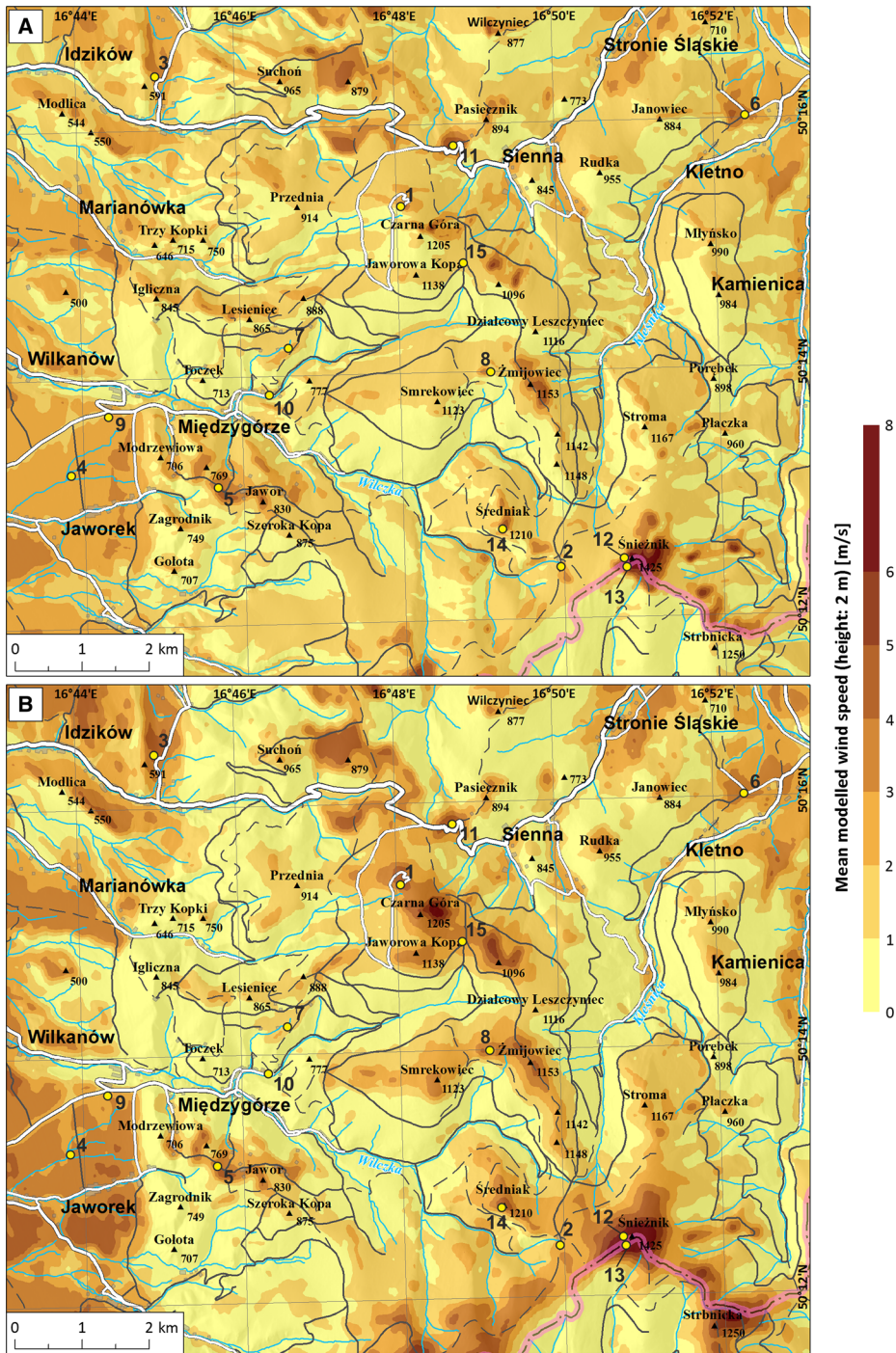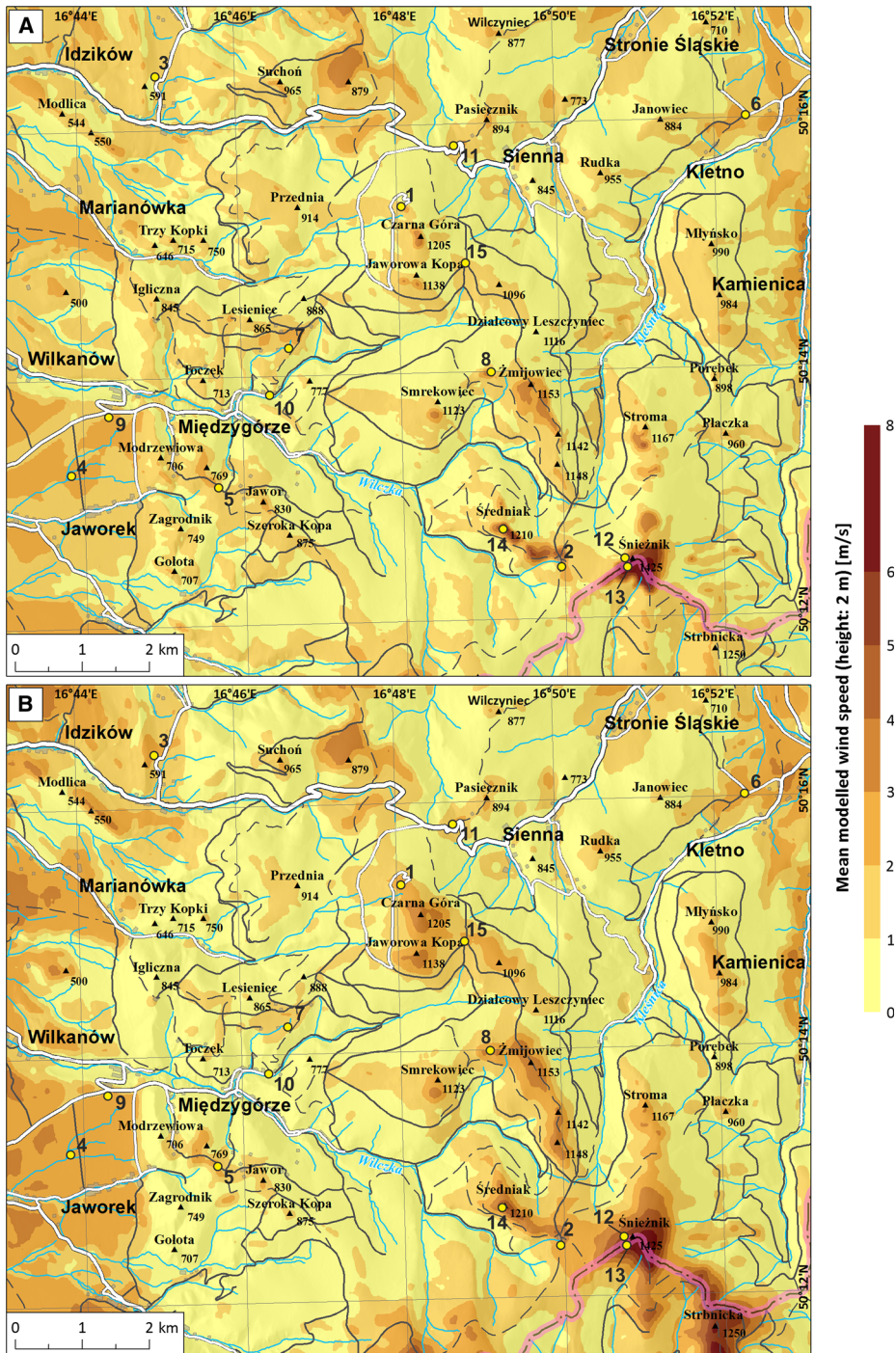
Figure 10
Spatial distribution of mean modeled wind velocity differences (ΔV) at height of 2 m above ground (26 May 2012; 13:00). The comparison concerns the following input roughness datasets: **a** CLC raster and CLC vector ($\Delta V = V_{CLCr} - V_{CLCv}$); **b** CLC raster and BDOT10k vector database ($\Delta V = V_{CLCr} - V_{BDOT10k}$). *Yellow dots* indicate measurement/validation points, *numbers* indicate point ID—see Tables 2 and 5
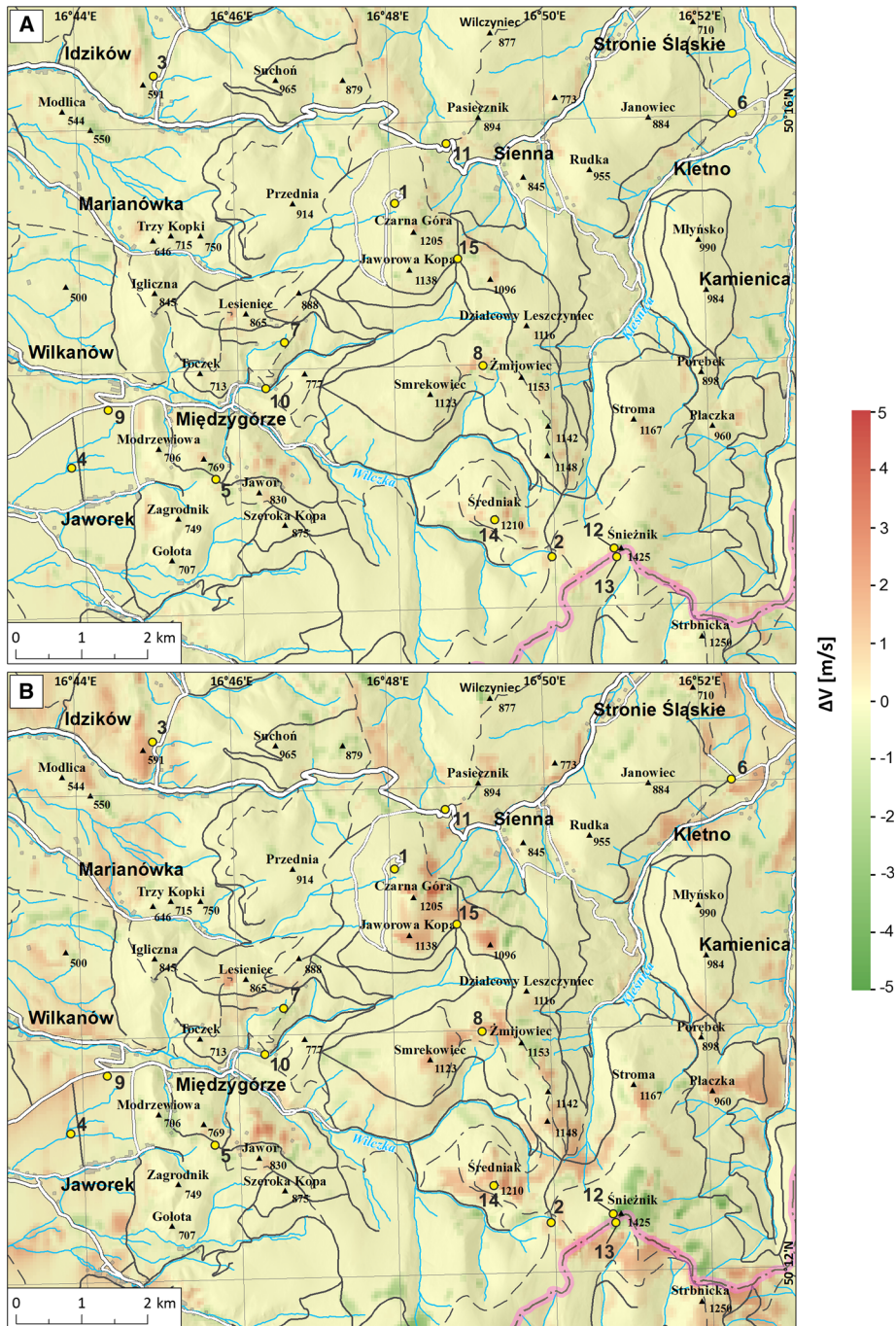
Figure 11

Spatial distribution of mean modeled wind velocity differences (ΔV) at height of 2 m above ground (26 May 2012; 13:00). The comparison concerns the following input roughness datasets: **a** CLC raster and LiDAR-based DEM and DSM ($\Delta V = V_{CLCr} - V_{LiDAR}$); **b** BDOT10k vector database and LiDAR-based DEM and DSM ($\Delta V = V_{BDOT10k} - V_{LiDAR}$). *Yellow dots* indicate measurement/validation points, *numbers* indicate point ID—see Tables 2 and 5
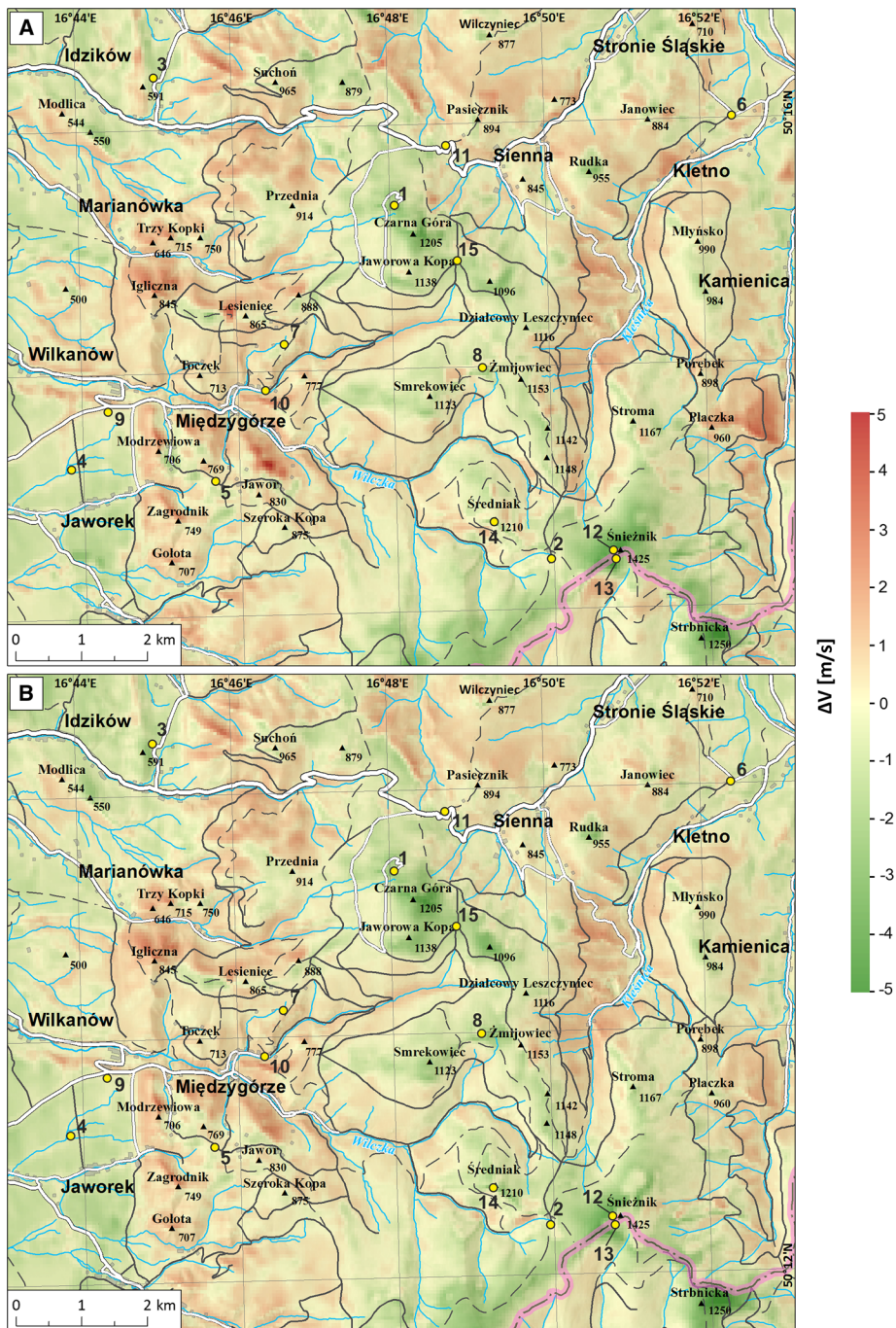
original BDOT10k land-use classes neglect "transitional woodland-shrub" CLC category, thus sparse coniferous forests (typical land coverage for these altitudes in the Śnieżnik Massif and the whole Sudetes range) are not represented properly. On the other hand, BDOT10k data were accurate enough to reflect the effects of linear obstacles such as trees and bushes along the roads (e.g. a road leading westwards from Międzygórze—Fig. 10b; see also Fig. 2) and small vegetation canopies in foothill areas (e.g. NW part of the area, near Idzików) (Fig. 10b). Moreover, the distribution of velocity above the Śnieżnik dome is completely different, comparing to CLC-based results. This is caused by more realistic roughness approximation due to avoidance of relief-induced errors, as mentioned by JANCEWICZ (2014).

The wind-field modeled with use of LiDAR data distinguishes itself by much higher velocity values at high altitudes and relatively low velocities in densely forested valleys (Figs. 8, 9, 11). This is an effect of roughness data continuity which reflect details of spatial variability of vegetation height inside the canopies (Fig. 6).

The analysis of model performance indices enables a more detailed insight into model's performance with an application of the aforementioned roughness data. It is conspicuous that CLC_R, CLC_V and BDOT10k datasets result in overall underestimation of the wind velocity (Fig. 12) (Table 5), though 100 m resolution induces greater underestimation than 50 m, especially in case of CLC_V and BDOT10k. This is mostly caused by improper land cover classification nearby measurement/validation points (e.g. Śnieżnik 2; Mariańskie Skały, Żmijowa Polana). To the contrary, the LiDAR data result in overall overestimation of the velocity ($B_v = 0.11$ m/s within 100 m and 0.26 m/s within 50 m resolution).

In respect of $RMSE_v$, Canyon model performed best while using the LiDAR-based roughness ($RMSE_v = 0.87$ and 0.80 m/s for 100 and 50 m resolution). BDOT10k and CLC_V induced relatively similar results (respectively: 1.41 and 1.42 m/s for 100 m grid; 1.09 and 1.15 m/s for 50 m grid), while the highest error value characterized the CLC_R output (1.47 for 100 m and 1.33 for 50 m grid) (Table 5; Fig. 12). These changes of mean error values might be caused by emergence of some roughness details,

which were "sub-grid" in lower resolution—land-use data are especially fragile to this type of effects due to the their qualitative character. However, this cannot be univocally stated within the presented experimental setup and should be a subject of further investigation. The detailed review of B_v and $RMSE_v$ for particular validation points (Table 5) reveals that the biggest differences between the results obtained with different roughness datasets appear at Śnieżnik 2 and Mariańskie Skały locations. In the first case CLC data lead to considerable underestimation of velocity (up to -5.6 m/s in 50 m grid), BDOT10k results fitted better (-1.2 m/s), while LiDAR-based results tend to slightly overestimate it (0.4 m/s). The case of Mariańskie Skały was similar—only LiDAR dataset provided roughness information which could make Canyon solve properly for this station. In this case, the pre-classified land-use data do not give a proper approximation of the pattern of roughness elements nearby the measurement point. The big improvement of model's performance due to the growing number of roughness details could be also observed at Żmijowa Polana, Jaworek, and Idzików. On the other hand, at Czarna Góra site, the use of LiDAR data caused a noticeable overestimation of velocity. This single case implies conjecture of roughness underestimation—it can be caused by the value of porosity factor which might be unfitting for the predominant shapes of trees' crowns at this altitude. Finally, the most disturbing case is Śnieżnik 1 point, which is characterized by high velocity overestimation regardless of the input roughness data. This may be caused by a local change of atmospheric stability (shallow stable layer), which might have led to decrement of wind velocity—if so, this problem cannot be solved using mean parameterization for atmospheric stability inside the whole calculation domain. Unfortunately, there is no undeniable proof that the aforementioned meteorological conditions actually appeared, thus this explanation should only be treated as a possibility.

According to the aforesaid observations, the LiDAR data appeared to induce the best Canyon performance. An additional application of the direction-dependent roughness parameter (h_{ceff}), applied only for 50 m grid, resulted in further minor decrement of the error values (Table 6). For instance, the
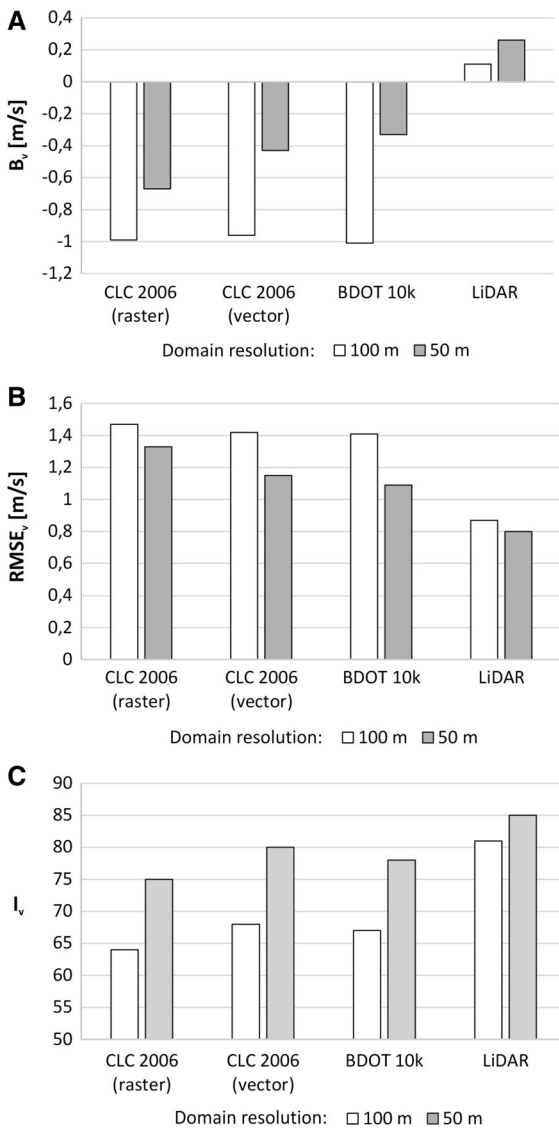
Figure 12
Impact of the particular roughness datasets on the overall values of wind velocity modeling performance indices: **a** mean B_v, **b** mean $RMSE_v$, **c** mean I_v

mean $RMSE_V$ decreased by 0.04 m/s comparing to the "standard" h_c. This error measure also did not change more than ±0.2 m/s in any measurement point. Figure 13 provides the best illustration of the subtlety of changes in the modeled velocity field. Nonetheless, h_{ceff}-based results are characterized by the mean B_v value of 0.17 m/s, which indicates that the overall tendency to overestimate wind velocity is slightly lower.

Comparing to the previous study at the Śnieżnik Massif test site, the overall performance of the model was improved. The mean $RMSE_V$ value was reduced from 1.0 m/s (Jancewicz 2014) to little less than 0.8 m/s, while the mean I_v value increased from 82 to 85 (Table 7). However, in this study a different elevation model was used than in the previous study.

Probably, there is a possibility to achieve further improvements of model's performance, as the LiDAR data offer such a high level of details that could be used in the process of roughness parameterization. However, a certain part of generated errors may be a consequence of solver's limitations.

5. Summary

This study demonstrates that the near-ground diagnostic wind velocity modeling in mountainous terrain (with an assumption of atmospheric neutral stability and relatively constant wind conditions) needs to be supported by apt roughness information. The use of LiDAR-based input roughness dataset improves performance of the diagnostic model, comparing to the qualitative datasets. It is distinctly expressed by calculated error indices. Moreover, the change of grid resolution from 100 m up to 50 m adjusts further model's performance. A slight improvement can be accomplished while modeling with use of re-calculated "windward" roughness values. One can observe that, while using various input qualitative data, the differences between calculated wind-velocity fields are caused by interference of following key factors: data properties (format and spatial resolution) and land-use classification.

These observations lead to a major conclusion that roughness information pre-processing should be inevitably considered in relation to the qualities of the available datasets.

On one hand there are pre-classified land coverage sets which provide categorical information, hence the estimated roughness is discrete. In consequence, roughness information may contain errors due to.

(a) Insufficient number of land cover classes.
(b) Inappropriate roughness values assignment.

Table 5

Roughness values and mean error measures of wind velocity calculated for particular validation points, considering the results of using different input roughness datasets in the wind velocity modeling within 100 and 50 m grid resolution

			ID	1 Czarna Góra	2 Hala pod Śnieżnikiem	3 Idzików	4 Jaworek	5 Jaworek Górny	6 Kletno	7 Łąki Myśliwskie	8 Mariańskie Skały
			Roughness dataset								
Domain resolution —100 m	*Roughness*	h_c (m)	CLC (raster)	9.3	2.7	0.7	0.2	0.2	0.7	9.3	2.7
			CLC (vector)	9.3	2.7	0.7	0.2	0.2	0.7	0.2	2.7
			BDOT 10k	9.3	9.3	0.2	0.2	0.2	0.2	0.2	9.3
			LiDAR	1.9	0.4	0.0	0.1	0.3	0.4	1.1	1.2
	Error measure	B_v (m/s)	CLC (raster)	−1.2	−1.3	−1.1	−0.7	0.1	−0.1	−1.5	−2.2
			CLC (vector)	−1.2	−1.5	−1.2	−0.6	0.2	−0.1	−0.8	−2.1
			BDOT 10k	−1.0	−1.0	−1.0	−0.9	0.2	−0.4	−0.3	−3.3
			LiDAR	1.3	−0.4	−0.2	−0.7	0.4	−0.4	−0.3	−1.0
		$RMSE_v$ (m/s)	CLC (raster)	1.2	1.3	1.2	0.8	0.5	0.2	1.6	2.2
			CLC (vector)	1.2	1.5	1.2	0.8	0.5	0.2	1.1	2.2
			BDOT 10k	1.0	1.0	1.0	1.0	0.5	0.4	0.8	3.3
			LiDAR	1.3	0.5	0.3	0.8	0.6	0.4	0.8	1.0
		I_v	CLC (raster)	57	67	78	88	91	97	38	54
			CLC (vector)	57	61	77	89	91	94	66	55
			BDOT 10k	64	76	81	83	91	95	73	16
			LiDAR	71	91	95	88	90	94	73	83
Domain resolution – 50 m	Roughness	h_c (m)	CLC (raster)	9.3	2.7	0.7	0.2	0.2	0.7	9.3	2.7
			CLC (vector)	9.3	2.7	0.7	0.2	0.2	0.7	0.2	2.7
			BDOT 10k	9.3	0.2	0.2	0.2	0.2	0.2	0.2	9.3
			LiDAR	3.0	0.2	0.0	0.0	0.3	0.2	0.3	0.4
	Error measure	B_v (m/s)	CLC (raster)	−0.3	−0.9	−1.3	−1.1	0.4	−0.3	−1.0	−1.6
			CLC (vector)	−0.3	−0.8	−1.4	−1.1	0.4	−0.3	−0.1	−1.2
			BDOT 10k	0.3	−0.3	−1.3	−1.4	0.3	−0.2	0.1	−2.9
			LiDAR	1.3	−0.1	−0.6	−0.6	0.1	0.1	−0.4	−0.3
		$RMSE_v$ (m/s)	CLC (raster)	0.3	0.9	1.3	1.2	0.5	0.3	1.2	1.6
			CLC (vector)	0.3	0.8	1.4	1.2	0.5	0.3	0.7	1.3
			BDOT 10k	0.3	0.4	1.3	1.4	0.5	0.3	0.7	2.9
			LiDAR	1.3	0.3	0.7	0.8	0.4	0.3	0.8	0.4
		I_v	CLC (raster)	91	80	72	79	92	96	65	68
			CLC (vector)	91	80	70	79	92	96	79	78
			BDOT 10k	92	93	74	73	93	97	79	31
			LiDAR	71	96	89	89	92	96	71	94

Table 5

continued

		ID Roughness dataset	9 Międzygórze 1	10 Międzygórze 2	11 Puchaczówka	12 Śnieżnik 1	13 Śnieżnik 2	14 Średniak	15 Żmijowa Polana	Mean value
Domain resolution —100 m	*Roughness* h_c (m)	CLC (raster)	*0.2*	*9.3*	*0.2*	*0.3*	*9.3*	*2.7*	*9.3*	–
		CLC (vector)	*0.2*	*2.7*	*0.2*	*0.3*	*2.7*	*2.7*	*9.3*	–
		BDOT 10k	*0.2*	*0.2*	*0.2*	*0.3*	*0.2*	*2.7*	*9.3*	–
		LiDAR	*0.2*	*5.5*	*0.1*	*0.0*	*0.0*	*0.5*	*2.6*	–
	Error measure B_v (m/s)	CLC (raster)	0.9	–1.1	–0.1	1.7	–4.1	–2.0	–2.2	–0.99
		CLC (vector)	0.9	–1.0	–0.1	**1.4**	–4.6	–2.0	–1.7	–0.96
		BDOT 10k	0.5	**–0.9**	–0.2	**1.4**	–3.4	–2.6	–2.3	–1.01
		LiDAR	**0.4**	–1.1	**–0.1**	3.6	**0.3**	**0.0**	**–0.2**	**0.11**
	$RMSE_v$ (m/s)	CLC (raster)	0.9	1.2	**0.6**	1.8	4.1	2.2	2.2	1.47
		CLC (vector)	0.9	1.1	**0.6**	**1.5**	4.6	2.2	1.7	1.42
		BDOT 10k	0.6	**0.9**	0.7	**1.5**	3.4	2.7	2.3	1.41
		LiDAR	**0.4**	1.2	**0.6**	3.7	**0.3**	**0.9**	**0.3**	**0.87**
	I_v	CLC (raster)	77	24	**86**	70	56	66	16	64
		CLC (vector)	77	39	**86**	**74**	49	65	41	68
		BDOT 10k	85	**49**	85	**74**	66	51	11	67
		LiDAR	**89**	24	**86**	46	**97**	**88**	**92**	**81**
Domain resolution – 50 m	Roughness h_c (m)	CLC (raster)	*0.2*	*9.3*	*0.2*	*0.3*	*9.3*	*2.7*	*9.3*	–
		CLC (vector)	*0.2*	*4.0*	*0.2*	*0.3*	*2.7*	*2.7*	*9.3*	–
		BDOT 10k	*0.2*	*4.0*	*0.2*	*0.3*	*0.1*	*2.7*	*9.3*	–
		LiDAR	*0.1*	*1.0*	*0.1*	*0.0*	*0.0*	*0.2*	*2.8*	–
	Error measure B_v (m/s)	CLC (raster)	**0.1**	–0.6	**0.2**	3.0	–5.6	0.4	–1.5	–0.67
		CLC (vector)	**0.1**	**–0.3**	0.3	**2.9**	–4.1	0.5	–1.1	–0.43
		BDOT 10k	–0.2	**–0.3**	0.3	3.3	–1.2	**0.2**	–1.6	–0.33
		LiDAR	0.2	–0.6	**0.2**	3.4	**0.4**	0.9	**0.1**	**0.26**
	$RMSE_v$ (m/s)	CLC (raster)	**0.2**	0.6	**0.6**	**3.0**	5.6	1.2	1.5	1.33
		CLC (vector)	**0.2**	0.4	**0.6**	**3.0**	4.1	1.3	1.1	1.15
		BDOT 10k	0.4	**0.3**	0.7	3.3	1.2	**1.1**	1.6	1.09
		LiDAR	**0.2**	0.6	0.7	3.4	**0.4**	1.4	**0.4**	**0.80**
	I_v	CLC (raster)	94	72	87	53	32	86	50	75
		CLC (vector)	**96**	86	**88**	**54**	57	86	68	80
		BDOT 10k	89	**89**	**88**	50	90	**87**	45	78
		LiDAR	**96**	72	86	49	**97**	84	**92**	**85**

Bold font indicates the lowest error values

Italic values indicate roughness values

Table 6

Mean error measures calculated for particular validation points, considering results of modeling with use of standard LiDAR−based roughness and its "windward" modification

Station name	Czarna Góra	Hala pod Śnieżnikiem	Idzików	Jaworek	Jaworek Górny	Kletno	Łąki Myśliwskie	Mariańskie Skały
B_v								
LiDAR	1.3	**−0.1**	**−0.6**	−0.6	0.1	0.1	−0.4	**−0.3**
LiDAR (windward)	**1.2**	−0.2	−0.7	−0.6	**0.0**	**0.0**	**−0.3**	−0.4
$RMSE_v$								
LiDAR	1.3	0.3	**0.7**	0.8	0.4	0.3	0.8	**0.4**
LiDAR (windward)	**1.2**	0.3	0.8	0.8	**0.3**	**0.2**	0.8	0.5
I_v								
LiDAR	71	96	**89**	89	92	96	71	**94**
LiDAR (windward)	**73**	96	87	89	**94**	**97**	**73**	93

Station name	Międzygórze 1	Międzygórze 2	Puchaczówka	Śnieżnik 1	Śnieżnik 2	Średniak	Żmijowa Polana	Mean value
B_v								
LiDAR	0.2	−0.6	0.2	3.4	0.4	0.9	0.1	**0.26**
LiDAR (windward)	**−0.1**	−0.6	**−0.1**	3.4	**0.0**	0.7	0.1	**0.17**
$RMSE_v$								
LiDAR	0.2	0.6	**0.7**	**3.4**	0.4	1.4	0.4	**0.80**
LiDAR (windward)	0.2	0.6	0.7	3.5	**0.0**	1.2	**0.3**	**0.76**
I_v								
LiDAR	**96**	72	86	49	97	84	92	**84.9**
LiDAR (windward)	94	72	86	49	**100**	**86**	**93**	85.4

Bold font indicates the lowest error values

(c) Method of data collecting.

Accordingly, qualitative data have to be thoroughly analyzed (and corrected if necessary) before being used as a source of an input roughness information. Then, these datasets can provide a valuable improvement of model's performance, to be used consistently with previous experience with empirical roughness length estimation and classification.

On the other hand, high-resolution LiDAR-based continuous elevation data offer plenty of possibilities during the pre-processing stage. It is possible to prepare a roughness dataset which is suitable for any grid resolution. Furthermore, the continuous quantitative datasets seem to be exceptionally interesting within the scope of the optimization of "effective roughness length" calculation process. Accordingly, there are numerous issues which should be examined in an experimental way:

(a) Calculation of roughness inside the windward fan.
(b) Spatially variable canopy porosity.
(c) Application of solutions used in the modeling of wind fields in urban areas.
(d) Sub-grid effects induced by micro relief.

Thus, it seems that it is still possible to refine the roughness estimation process which may lead to further improvements of diagnostic wind-velocity modeling.

Figure 13

Spatial distribution of mean modeled wind velocity differences (ΔV) at height of 2 m above ground (26 May 2012; 13:00). The comparison concerns two methods of LiDAR-based roughness parameterization: mean height inside grid cell (h_c) and mean height inside windward-placed fan of 200 m radius ($h_{c \text{ eff}}$) − ($\Delta V = V_{hc} − V_{hc\text{eff}}$). *Yellow dots* indicate measurement/validation points, *numbers* indicate point ID—see Tables 2 and 5

Table 7

Comparison of Canyon CFD solver performance indices calculated for various test sites

Test site	Poiares Region (LOPES 2003)	Trevim Region (LOPES 2003)	Śnieżnik Massif (constant roughness) (JANCEWICZ 2014)	Śnieżnik Massif [CLC 2006 (2011) roughness] (JANCEWICZ 2014)	Śnieżnik Massif (LiDAR-based roughness)
Mean I_v	56	41	71	80	**85**

Appendix

See Table 8.

Table 8

Davenport classification of terrain roughness (WIERINGA et al. 2001)

z_0 (m)	Landscape description
0.0002 "Sea"	Open sea or lake (irrespective of wave size), tidal flat, snow-covered flat plain, featureless desert, tarmac and concrete, with a free fetch of several kilometres
0.005 "Smooth"	Featureless land surface without any noticeable obstacles and with negligible vegetation; e.g. beaches, pack ice without large ridges, marsh and snow-covered or fallow open country
0.03 "Open"	Level country with low vegetation (e.g. grass) and isolated obstacles with separations of at least 50 obstacle heights; e.g. grazing land without wind breaks, heather, moor and tundra, runway area of airports. Ice with ridges across-wind
0.10 "Roughly open"	Cultivated or natural area with low crops or plant covers, or moderately open country with occasional obstacles (e.g. low hedges, isolated low buildings or trees) at relative horizontal distances of at least 20 obstacle heights
0.25 "Rough"	Cultivated or natural area with high crops or crops of varying height, and scattered obstacles at relative distances of 12–15 obstacle heights for porous objects (e.g. shelterbelts) or 8–12 obstacle heights for low solid objects (e.g. buildings)
0.5 "Very rough"	Intensively cultivated landscape with many rather large obstacle groups (large farms, clumps of forest) separated by open spaces of about eight obstacle heights. Low densely-planted major vegetation like bush land, orchards, young forest. Also, area moderately covered by low buildings with interspaces of 3–7 building heights and no high trees
1.0 "Skimming"	Landscape regularly covered with similar-size large obstacles, with open spaces of the same order of magnitude as obstacle heights; e.g. mature regular forests, densely built-up area without much building height variation
≥2.0 "Chaotic"	City centres with mixture of low-rise and high-rise buildings, or large forests of irregular height with many clearings

REFERENCES

ABBES, M., BELHADJ, J. (2012), *Wind resource estimation and wind park design in El-Kef region, Tunisia*, Energy *40*, 348–357.

CHO, J., MIYAZAKI, S., YEH, P.J.-F., KIM, W., KANAE, S., OKI T. (2012), *Testing the hypothesis on the relationship between aerodynamic roughness length and albedo using vegetation structure parameters*, International Journal of Biometeorology *56*, 411–418.

COLIN, J., FAIVRE, R. (2010), *Aerodynamic roughness length estimation from very high-resolution imaging LIDAR observations over the Heihe basin in China*, Hydrology and Earth System Sciences *14*, 2661–2669.

Corine Land Cover 2006 raster dataset (version 15) (2011); http://www.eea.europa.eu/data-and-maps/data/corine-land-cover-2006-raster-1. Accessed date 13 Mar 2012.

Corine Land Cover 2006 vector dataset (version 17) (2013); http://www.eea.europa.eu/data-and-maps/data/clc-2006-vector-data-version-3. Access date 20 Mar 2014.

Database of Topographical Objects (BDOT10k)—vector database; http://www.codgik.gov.pl/index.php/zasob/baza-danych-obiektow-topograficznych.html. Accessed date 30 May 2015.

DAVENPORT, A.G. (1960), *Rationale for determining design wind velocities*, Journal of Structural Division *86*, 39–68.

DE MEIJ, A., VINUESA, J.F. (2014), *Impact of SRTM and Corine Land Cover data on meteorological parameters using WRF*, Atmospheric Research *143*, 351–370.

DONG, Z., GAO, S., FRYREAR, D.W. (2001), *Drag coefficients, roughness length and zero-plane displacement height as disturbed by artificial standing vegetation*, Journal of Arid Environments *49*, 485–505.

EMEIS, S., KNOCHE, H.R., Applications in meteorology. In Geomorphometry: concepts, software, applications. (eds. Hengl T., Reuter H. I.) (Elsevier 2007) pp. 603–623.

EMERY, C., TAI, E., YARWOOD, G., Enhanced meteorological modeling and performance evaluation for two Texas ozone episodes. (ENVIRON International Corporation, 2001).

GARRATT, J.R., The atmospheric boundary layer (Cambridge, New York, 1994).

GRIMMOND, C.S.B., OKE, T.R. (1999), *Aerodynamic properties of urban areas derived from analysis of surface form*. Journal of Applied Meteorology *38*, 1262–1292.

HAMMOND, D.S., CHAPMAN, L., THORNES, J.E. (2012), *Roughness length estimation along road transects using airborne LIDAR data,* Meteorological Applications *19*, 420–426.

HANSEN, F.V., Surface roughness lengths (Army Research Laboratory, 1993).

HASAGER, C.B., NIELSEN, N.N., JENSEN, N.O., BOEGH, E., CHRISTENSEN, J.H., DELLWIK, E., SOEGAARD, H. (2003), *Effective roughness calculated from satellite-derived land cover maps and hedge-information used in a weather forecasting model*, Boundary-Layer Meteorology *109*, 227–254.

HEISLER, G.M., DE WALLE, D.R. (1988), *Effects of windbreak structure on airflow*, Agriculture, Ecosystems & Environment *22/23*, 41–69.

JACKSON, P.S. (1981), *On the Displacement Height in the Logarithmic Velocity Profile*, Journal of Fluid Mechanics *111*, 15–25.

JACOBSON, M.Z., Fundamentals of atmospheric modeling (University Press, Cambridge 2005).

JANCEWICZ, K. (2014), *Remote sensing data in wind velocity field modeling: a case study from the Sudetes (SW Poland),* Pure and Applied Geophysics *171*, 941–964.

JASINSKI, M.F., CRAGO, R.D. (1999), *Estimation of vegetation aerodynamic roughness of natural regions using frontal area density determined from satellite imagery*, Agricultural and Forest Meteorology *94*, 65–77.

JIMENEZ, P.A., DUDHIA, J. (2012), *Improving the representation of resolved and unresolved topographic effects on surface wind in the WRF model*, Journal of Applied Meteorology and Climatology, *51*(2), 300–316.

LOPES, A.M.G. (2003), *WindStation—a software for the simulation of atmospheric flows over complex topography*, Environmental Modeling & Software *18*, 81–96.

LOPES, A.M.G. (2013), WindStation 3.1.0: User's Manual.

MORALES, L., LANG, F., MATTAR, C. (2012), *Mesoscale wind speed simulation using CALMET model and reanalysis information: An application to wind potential,* Renewable Energy *48*, 57–71.

PIASECKI, J., Wybrane cechy klimatu Masywu Śnieżnika, In Masyw Śnieżnika. Zmiany w środowisku przyrodniczym (eds. JAHN A., KOZIOWSKI S., PULINA M.) (PAE, Warszawa 1996) pp. 189–206.

PIASECKI, J., SAWIŃSKI, T., The Niedźwiedzia Cave in the climatic environment of the Kleśnica Valley (Śnieżnik Massif), In Karst of the Częstochowa Upland and of the Eastern Sudetes: palaeoenviroments and protection (eds. STEFANIAK K., TYC A., SOCHA P.) (University of Silesia, Sosnowiec – Wrocław 2009) pp. 423–454.

PLATE, E.J., Engineering meteorology (Elsevier, New York, 1982).

RAMLI, N.I., IDRIS ALI, M., SAAD, M.S.H., MAJID, T.A (2009), Estimation of the roughness length (z_o) in malaysia using satellite image, Conference Proceedings of The Seventh Asia-Pacific Conference on Wind Engineering, http://www.iawe.org/Proceedings/7APCWE/T2D_1.pdf.

SCHAUDT, K.J., DICKINSON, R.E. (2000), *An approach to deriving roughness length and zero-plane displacement height from satellite data, prototyped with BOREAS data*, Agricultural and Forest Meteorology *104*, 143–155.

SILVA, J., RIBEIRO, C., GUEDES, C. (2007), Roughness length classification of Corine Land Cover Classes, Conference Proceedings of European Wind Energy Conference 2007, http://www.ewea.org/ewec2007/allfiles2/545_Ewec2007fullpaper.pdf.

SUDER, A., SZYMANOWSKI, M. (2014), *Determination of ventilation channels in urban area: a case study of Wrocław (Poland)*, Pure and Applied Geophysics *171*, 965–975.

TAYLOR, P.A. (1987), *Comments and further analysis of effective roughness lengths for use in numerical three-dimensional models*, Boundary-Layer Meteorology *39*, 403–418.

THOM, A.S. (1971), *Momentum absorption by vegetation*, Quarterly Journal of Royal Meteorological Society *97*, 414–428.

TIAN, X., LI, Z.Y, VAN DER TOL, C., SU, Z., LI, X., HE, Q.S., BAO, Y.F., CHEN, E.X., LI, L.H. (2011), *Estimating zero-plane displacement height and aerodynamic roughness length using synthesis of LiDAR and SPOT-5 data,* Remote Sensing of Environment *115*, 2330–2341.

TRUHETZ, H., High resolution wind field modeling over complex topography: analysis and future scenarios. (Wegener Center for Climate and Global Change, Scientific Report No. 32-2010, Graz 2010).

WIERINGA, J. (1993), *Representative roughness parameters for homogenous terrain*, Boundary-Layer Meteorology *63*, 323–363.

WIERINGA, J., DAVENPORT, A.G., GRIMMOND, C.S.B., OKE, T.R. (2001) New revision of Davenport roughness classification. Proceedings of the 3rd European & African Conference on Wind Engineering.

WOOD, N., BROWN, A.R., HEWER, F.E., (2001), *Parametrizing the effects of orography on the boundary layer: An alternative to effective roughness lengths*, Q. J. R. Meteorol. Soc., *127*(573), 759–777.

World Meteorological Organization, Guide to meteorological instruments and methods of observation, Tech. Rep. 8 (Seventh Edition). (Secretariat of World Meteorological Organization, Geneva 2008).

YAMAZAWA, H., KONDO J. (1989), *Empirical-statistical method to estimate the surface wind speed over complex terrain*, Journal of Applied Meteorology and Climatology *28*, 996–1001.